Title

Aberration corrected STEM by means of diffraction gratings

Authors

Linck, Martin

Ercius, Peter A

Pierce, Jordan S

et al.

Publication Date

2017-11-01

DOI

10.1016/j.ultramic.2017.06.008

Peer reviewed

Aberration Corrected STEM by means of Diffraction Gratings

Martin Linck[1], Peter A. Ercius[2], Jordan S. Pierce[3] and Benjamin J. McMorran[3]

1. Corrected Electron Optical Systems GmbH, Englerstr. 28, D-69126 Heidelberg, Germany.

2. National Center for Electron Microscopy, Molecular Foundry, Lawrence Berkeley National Laboratory, 1 Cyclotron Road, Berkeley CA 94720, United States.

3. Department of Physics, 1274 University of Oregon, Eugene OR 97403-1274, United States.

Abstract:

In the past 15 years, the advent of aberration correction technology in electron microscopy has enabled materials analysis on the atomic scale. This is made possible by complex arrangements of multipole electrodes and magnetic solenoids to compensate the aberrations inherent to any focusing element of an electron microscope. Here, we describe an alternative method to correct for the spherical aberration of the objective lens in a scanning transmission electron microscopy (STEM) using a passive, nanofabricated diffractive optical element. This holographic device is installed in the probe forming aperture of a conventional electron microscope and can be designed to remove arbitrarily complex aberrations from the electron's wave front. In this work, we show a proof of principle experiment that demonstrates successful correction of the spherical aberration in STEM by means of such a grating corrector (GCOR). Our GCOR enables us to record aberration-corrected high-resolution HAADF STEM images, although yet without any improvement in probe current and resolution.

Author Contact Information:

Dr. Martin Linck, CEOS GmbH, Englerstr. 28, D-69126 Heidelberg, Germany

Tel. +49-(0)6221-89467-258

Fax +49-(0)6221-89467-29

e-mail linck@ceos-gmbh.demailto:linck@ceos-gmbh.demailto:linck@ceos-gmbh.demailto:linck@ceos-gmbh.de

Highlights:

- Spherical aberration correction by means of an electron diffraction grating
- Ronchigram analysis of individual, diffracted beams
- High-resolution HAADF STEM imaging using a diffracted, aberration-corrected beam

Keywords:

Diffraction gratings; aberration correction; Cs-corrector; high-resolution STEM; Ronchigram

1. Introduction

Modern electron microscopy allows us to analyze our world at sub-nanometer length-scales. After correction of resolution-limiting spherical aberration became feasible several years ago [1,2], electron microscopy has developed into a tool to accurately determine atomic positions, local elemental composition, and bonding with very high precision [e.g. 3-7]. Aberration correctors can be used either post-specimen to improve image resolution and contrast in transmission electron microscopy (TEM) [1] or pre-specimen to produce a more sharply focused probe for scanning transmission electron microscopy (STEM) [2,8].

Aberration correctors consist of precise arrangements of multiple electrodes and magnetic solenoids, each of which must be supplied with well-controlled, highly-stable voltages and currents [9]. Proper use of an aberration corrected microscope requires time for alignment, and the fully corrected state is only valid for relatively short periods of time [10] although practical sub-Ångstrom imaging is possible for hours with small corrections applied manually by the operator. State-of-the-art aberration correctors are a feat of human engineering, and they are now used as a critical electron optical component to provide unprecedented analysis of structure at the atomic scale with sub-Angstrom resolution. However, they are quite expensive (adding a significant amount to the base cost of an electron microscope) and require additional training for proper usage. Here, we describe an alternative method of compensating for the spherical aberration inherent to round magnetic lenses by using a single passive component that is installed in the existing probe forming aperture assembly of any conventional STEM. We demonstrate spherical aberration correction using a nanofabricated diffraction grating [11,12]. The setup is used to record aberration-corrected HAADF STEM images of a silicon sample.

Beginning with early work by Brown and Lohmann [13], computer-designed holograms used as diffractive optics have become a common tool for controlling the phase and amplitude of light [14]. Pioneering work has also already been performed in electron optics [15-17]. Electron diffraction gratings became particularly popular to the electron microscopy community when Verbeeck et al. and McMorran et. al. reported on the creation of electron vortex beams by means of a fork-dislocation diffraction grating [18,19]. The idea was adapted from light optics [20-22] after preliminary work with electron beams had predicted this effect [23]. This kind of “wavefront engineering” has already been used to produce arbitrary phase structures in both light [13,14] and electron beams [24-29]. In principle, this approach had also been used already for light-optical wave front reconstructions of early off-axis electron holograms [29b]. Most recently, nanoscale gratings were used in an electron microscope to measure electron-surface interactions [30,31], image the electric field around a charged tip [32], and to precisely measure the wavefront curvature of an electron beam [33] among many other examples.

2. Theory

2.1. Wavefront manipulation by diffraction gratings

A diffraction grating allows imprinting a phase shift Φ into the diffracted waves of an incident plane wave by superposing this phase shift Φ to the "empty", linear phase shift of a uniform line grating. Sign and magnitude of the imprinted phase shift of the diffracted electron waves Ψ_n are given by the diffraction order *n* as illustrated in Figure 1:

$$\Psi_n \sim \exp\{i \cdot n\Phi\}. \qquad (1)$$

This work utilizes electron-transparent silicon nitride membranes which can be considered a weak-phase object for high-energy electrons. Since electron waves have significantly smaller wavelengths compared to light, diffraction gratings for electrons require patterning capabilities with nanometer accuracy over micron length scales as provided e.g. by focused ion-beam (FIB) preparation tools [27,28].

In terms of diffraction efficiency two important aspects have to be taken into account. Firstly, the structure has to transmit as many electrons a possible. Secondly, as many of the remaining electrons as possible have to be diffracted into the desired diffraction order. These requirements can be quantified by the grating's transmittance

$$\eta_{abs} = I_{trans} / I_{tot} = \sum_k I_{(k)} / I_{tot}\,. \quad (1b)$$

with the total incident and transmitted beam intensities I_{tot} and I_{trans}, respectively, where the transmitted intensity I_{trans} is the sum of all individual diffracted beams of intensities $I_{(k)}$. The relative and absolute diffraction efficiencies into diffraction orders *k* are expressed by

$$\eta_{rel,(k)} = I_{(k)} / I_{trans} \quad \text{and} \quad \eta_{abs,(k)} = I_{(k)} / I_{tot}\,, \qquad (1c)$$

respectively. By accurately tuning the shape of the grating lines within such a diffraction grating, the beam intensity of particular diffraction order can be maximized or – if needed – even be suppressed [28].

Very high diffraction efficiencies for a particular diffraction order have been reported already [27, 28]. Here, we used a grating with a very cosine-alike thickness modulation of the grating lines; this allows restricting further considerations to diffraction orders $|n| \leq 1$. In subsequent discussions, we ignore all diffraction orders $|n| > 1$ for simplicity due to their suppressed, relatively weak intensity.

2.2. Diffraction gratings in a STEM

According to Fourier optics [e.g. 34], an electron diffraction grating with a phase shift $\Phi(R)$ and the line spacing s centered in the plane of the probe forming aperture will create a series of STEM probes at the plane of the object. R denotes the spatial coordinate in the condenser aperture with the origin at the optical axis.

The grating coordinate R can be translated into an incident illumination angle θ with respect to the object by taking into account the aperture magnification M_{ap} and the focal length f of the objective lens:

$$\theta = R \cdot M_{ap} / f \quad (2)$$

The aperture magnification M_{ap} is the factor by which the condenser lens system magnifies the probe forming aperture into the front focal plane of the objective lens (compare Figure 2).

In a similar way, the spatial separation d of the 0^{th} and 1^{st} order diffracted STEM probes can be derived from the line spacing s of the grating. The diffraction angle in the plane of the grating results as $\beta = \lambda/s$ and demagnifies into the front focal plane of the objective lens as $\beta' = \beta/M_{ap}$. Thus, in the object plane a 1^{st} order diffracted probe is then displaced from the undiffracted probe by

$$d = \lambda / s \cdot f / M_{ap} . \quad (3)$$

For the diffracted probes the edge of the grating acts as a sharp aperture because the grating lines abruptly stop at a certain radius R. Therefore, the probe angle of the diffracted probes is strictly determined by the radius R of the circular grating. In general, the grating can also be designed such that the grating lines softly radially vanish to create e.g. Gaussian beams [29,12]. In practice, the transmitted, 0^{th}-order probe, however, is not limited by the grating edge because of general transparency of the unpatterned silicon nitride film. Fortunately, some modern microscopes have an additional condenser aperture between the probe-forming aperture and the objective lens, which can be used to effectively limit the center probe to a similar probe angle as the +/-1 order beams.

Although the STEM probe is scanned over the sample in the object plane, the primary STEM signals of this sample are detected in a diffraction plane below the object plane. Therefore, the diffraction patterns of the multiple STEM probes generated by the grating are superimposed over each other. As an example, the three Ronchigrams of the 0^{th} order probe and the diffracted probes of order +/-1 cannot be observed individually e.g. for accurate STEM alignment of a particular probe. This would require an additional aperture in an intermediate image plane in between the diffraction grating and the object plane which does not exist in most microscopes at conventional settings. However, one of the three superposed Ronchigrams can be selected in the first image plane behind the object using the selected area (SA) aperture. Subsequently, the Ronchigrams of this individual diffracted probe can be observed separately, as illustrated in Figure 3. This approach, however, does not work for most other detectable STEM signals. The high angle scattering for the HAADF signal, for example, is heavily delocalized in the

image plane due to the image-side objective lens aberrations, and thus cannot be separated by means of the SA aperture. Moreover, secondary signals such as EDX which are detected above the sample cannot be separated at all without an additional aperture in the probe-forming optics. The only exception is a carefully selected sample geometry: an object area close to the sample edge or a nano-pillar-shaped object can be illuminated such that only the first-order diffracted probe interacts with the sample. This approach, however, is restricted to object areas which are closer to the sample's edge than the separation distance *d* of the probes.

2.3. Gratings for aberration correction

The effect of blurring a STEM probe due to spherical aberration can be described by means a virtual phase plate $\exp\{-i\,\chi_{OL}\}$ with

$$\chi_{OL} = \frac{2\pi}{\lambda} \cdot \frac{C_3}{4} \theta^4 \qquad (4)$$

that is located in the probe forming aperture above the objective lens [34]. Here, λ denotes the electron's wave length (1.969 pm for 300 keV-electrons), $C_3 = C_S$ the coefficient of the dominating third order spherical aberration, and θ the angle, i.e. the illumination direction. For the purpose of correcting this spherical aberration in a STEM, the diffraction grating centered in the plane of the probe forming aperture has to create a first-order diffracted wave with a radially-dependent phase shift opposite to the one imposed by the objective lens. This requires a grating phase shift $\exp\{i\,\chi_G\}$ shaped as

$$\chi_G = c_G \cdot R^4, \qquad (5)$$

i.e. a radial fourth-order parabola, where c_G denotes the geometry constant of the grating. To completely eliminate the effect of spherical aberration in the STEM probe at the object plane, c_G of the grating is chosen such that the grating phase shift exactly matches the spherical aberration of the probe forming lens for a given focal length *f* and aperture magnification M_{ap}:

$$c_G = \frac{2\pi}{\lambda} \frac{C_3}{4} \left(\frac{M_{ap}}{f} \right)^4 . \qquad (6)$$

If the condenser optics is adapted to achieve a different probe convergence angle with the same aperture size, the resulting change of aperture magnification M_{ap} requires a modification of the grating constant c_G accordingly. Consequently, a given grating will only correct the spherical aberration for one particular illumination setup. Analogous to multipole correctors, the condenser lenses can be interpreted as the transfer lens system between diffraction grating and objective lens; these also have to be accurately setup in order to provide a C_S-corrected STEM probe.

The transmitted 0^{th} order beam is not affected by the phase shift of the grating, resulting in a conventional aberrated STEM probe at the plane of the sample. The positive first order (+1) beam, however, gains the grating phase shift χ_G, and the negative first order (-1) loses this phase shift. Consequently, in the "+1"-beam, the radial phase shift compensates the inherent spherical-aberration of the objective lens, resulting in an aberration-free STEM probe. For the "-1"-beam, the spherical aberration of the lens and the phase shift of the grating simply add up, resulting in an even larger spherical aberration and hence a very poor STEM probe in the specimen plane. Ideally, the diffracted beams of order 0 and -1 would be removed by means of a pre-specimen aperture to realize aberration-free STEM illumination with merely the +1 diffraction order.

3. Methods and Materials

3.1. Diffraction Grating

The diffraction grating used in these experiments was patterned on a commercially-available silicon nitride membrane, which is usually utilized as a support for TEM-samples. This thin film covers an area of 100 μm x 100 μm and has a thickness of 30 nm. An ultrathin layer of carbon minimizes charging effects. A FIB was used to pattern the membrane according to a binary template of trenches with alternating depth. Due to the Gaussian-like beam profile of the FIB, the binary image, i.e. a rectangular trench, results in a nearly cosine-shaped thickness profile. The depth profile can be used as a parameter to further optimize the diffraction efficiency of the grating [28].

To demonstrate aberration correction, we designed a grating of radius R_{max} = 35 μm for a probe illumination semi-angle of θ_{max} = 17.5 mrad (f/M_{ap} = 2 mm) and 300 keV electrons (λ = 1.969 pm). The corresponding grating constant results as c_G = 6.23 x 10^{-5} μm^{-4}. The grating line spacing s = 80 nm was chosen close to the performance limit of the focused ion beam instrumentation with a certain safety margin for reliable results. A detailed view of the diffraction grating is provided in Figure 4. The FFT of the SEM overview image allows extracting the geometric phase of the grating lines [e.g. 35]. Subsequent phase-unwrapping reveals a fourth order parabola, i.e. the expected shape of a spherical aberration.

3.2. Instrumental Setup

The GCOR was inserted into the second condenser (C2) probe forming aperture holder of an uncorrected FEI Titan 80-300 operated at 300 kV. The microscope's probe forming lens has a nominal spherical aberration value of C_3 = 1.25 mm. Using an aperture of radius R_{max} = 25 μm the probe's semi convergence angle was measured as θ_{max} = 12.5 mrad. The corresponding effective focal length of the probe-forming optics results as f/M_{ap} = 2 mm in this particular setting. To demonstrate the effect of

spherical aberration correction we purposefully chose a too-large aperture size, i.e. grating size, which yields a significantly too-large probe convergence angle for uncorrected STEM.

The grating's line spacing $s = 80$ nm determines a diffraction angle in the plane of the gratin of $\beta = 24.6$ µrad for the first order diffracted beams for 300 keV-electrons. Consequently, the corresponding probe separation d in the object plane can be estimated to 49.2 nm.

Ronchigram images were generated on a commercial holey carbon sample (Quantifoil). The selection of one of the three superposed Ronchigrams was achieved by means of the 10 µm SA-aperture as described in section 2.2. Each Ronchigram was recorded on the bottom-mounted Gatan US1000 CCD camera with 1 sec exposure time.

The high-resolution HAADF STEM images were acquired from a silicon sample in [110] orientation produced by in-situ FIB liftout. The HAADF angles were adjusted to 39 mrad and 200 mrad inner and outer angle, respectively. A long dwell time of 250 µs was needed due to the relatively low current in the "+1"-beam yielding a total acquisition time of about 79 sec for 512 x 512 pixels. With 30 pm pixel size the field of view results to about 15 x 15 nm^2.

4. Results and Discussion

4.1. Demonstration of spherical aberration correction

The experimental realization of three adjacent probes, i.e. the 0^{th} order probe symmetrically surrounded by the C_S-corrected "+1"-probe and the twice aberrated "-1"-probe, is shown in Figure 2. The probe separation d was measured as ~50 nm as predicted above. Evidently, diffraction orders $|n| > 1$ can be ignored due to negligible diffraction efficiencies. The transmittance of the grating amounts to $\eta_{abs} = 77.2\%$. Unfortunately, the diffracted beam intensities $I_{(\pm1)}$ have a relative diffraction efficiency of $\eta_{rel(\pm1)} = 3.3\%$ which reduces to an absolute diffraction efficiency $\eta_{abs(\pm1)} = 2.5\%$ for the first order diffracted beams. This is quite small compared to recent advances in grating manufacturing [27,28], hence there is significant room of improvement for future experiments. At the time the experiments had been performed we unfortunately were not able to measure the absolute beam currents. Therefore, we can only summarize the experimental diffraction efficiencies.

A real space image of the bright, Angstrom-sized probes, which reliably and directly shows the improved "sharpness" of the "+1"-probe, is very difficult to obtain in the TEM mode. Instead, the effect of spherical aberration and its correction is shown in the Ronchigrams following the suggested procedure of section 2.2. Figure 5 shows the isolated Ronchigrams of the C_S-corrected probe (+1), the transmitted probe (0) and the twice aberrated probe (-1) for the focused condition and about 125 nm STEM defocus in both, overfocus and underfocus direction. The unaffected 0^{th} order probe shows the well-known behavior of a Ronchigram under the presence of spherical aberration [36]: overfocus yields a heavily

distorted shadow image of the sample whereas underfocus produces concentric rings of infinite magnification. The corresponding in-focus Ronchigram only exhibits a very limited flat area in the Ronchigram center. The same basic behavior can be recognized in the deteriorated "-1"- probe though the related Ronchigram is much noisier due to the very limited probe current. Since the spherical aberration is twice as much compared to the 0th order, the flat surface in the focused Ronchigram is significantly smaller. Furthermore, the distortion of the object shadow in the overfocused Ronchigram has increased. Additionally, the radius of the concentric rings of infinite magnification at the same underfocus has become smaller since the same defocus has to counterbalance twice the spherical aberration. The behavior of the corrected "+1"-order Ronchigram, however, is much different: large overfocus and underfocus yield similar shadow images of the object. Moreover, the focused Ronchigram is widely flat over the whole size of the grating. The complete defocus series of the three probes covering a defocus range of at least 500 nm around Gaussian focus are provided as supplemental movies.

The present spherical aberration can be used to estimate the flat Ronchigram area, and vice versa. According to [36] the angle α representing the $\pi/4$-limit in the spherical aberration-affected Ronchigram can be estimated by

$$\alpha = 1.3\lambda^{1/4} C_3^{-1/4}. \qquad (7)$$

This estimation requires the defocus value C_1 to slightly counterbalance the C_3-effect with

$$C_1 = -0.71\lambda^{1/2} C_3^{1/2}. \qquad (8)$$

For the 0th order, unaffected Ronchigram and the "-1" order, twice-aberrated Ronchigram, the spherical aberrations of 1.25 mm and 2.5 mm yield $\pi/4$-angles of 8.2 mrad and 6.9 mrad, respectively. These angles can also be found experimentally as illustrated in the focused Ronchigrams of Figure 5. To estimate the remaining spherical aberration in the corrected probe, we reverse eq. (7). For a $\pi/4$-limit at the edge of the grating, i.e. 17.5 mrad, we find an upper C_3-limit of 0.06 mm, which is less than 5% of the nominal objective lens aberration.

For the transmitted 0th order beam (C_3 = 1.25 mm) and the twice-aberrated -1 order beam (C_3 = 2.5 mm) the circles of infinite magnification can be analyzed and compared to the angles $\alpha = (-C_1 / C_3)^{1/2}$. The procedure applied to our experimental Ronchigrams series (not shown here) confirms the above spherical aberration values, and moreover, verifies the defocus step size is consistent with angular calibration.

Much more elaborate methods for aberration measurement are widely used [37,38]. However, most of these methods incorporate a beam tilt. In contrast to multipole aberration correctors our corrector grating is positioned above the beam tilt coils. Therefore, in our case the beam tilt coils can only be used to align the axis of the grating to the axis of the objective lens, but not to tilt the beam w.r.t. both of the

components at the same time. In principle, this is analogous to the tilt coils between aberration corrector and objective lens which are mostly used as an alignment tool for axial coma to match the axis of corrector and objective lens. Figure 6 shows an example of a C_S-corrected Ronchigram with a displaced grating, i.e. a beam tilt between the grating and the objective lens inducing large axial coma.

The measurements and estimates above present a proof-of-principle experiment demonstrating the successful holographic correction of spherical aberration. Though our GCOR considerably improved the flat area of the Ronchigram, the corresponding angle still is small compared to the achievements of hardware aberration correctors [39-41]. Consequently, further residual aberrations such as star aberration or higher order astigmatisms are not (yet) realized.

4.2. Aberration-corrected HAADF STEM

In our STEM setup, the three adjacent probes are scanned simultaneously. Since the probes are separated by d = 50 nm, a HAADF STEM image generated by all three probes will comprise a superposition of three STEM images that are shifted w.r.t. each other by the distance d. Ideally, the object is positioned such that only the scan area of +1 probe covers the sample so that high-angle scattering signals that are collected on the HAADF detector can be solely attributed to the aberration-corrected STEM probe. If the object is shifted further onto the optical axis, the 0^{th} order STEM probe will also interact with the sample edge and contribute to the HAADF signal. In order to extract the HAADF signal of the aberration-corrected probe only, we chose the scan area to be small compared to the probe separation d and placed the SAD aperture such that the scan area of the aberration-corrected probe is isolated from the other scan areas. Although high-angle scattering is strongly delocalized in the plane of the selected area aperture, an acceptable isolation of the signal stemming from the aberration-corrected probe can be achieved. Figure 7 illustrates the experimental geometry and shows the corresponding HAADF STEM result. The STEM image of the holographically-corrected +1 order probe is very noisy due to its very limited probe current. Consequently, the lattice reflections in the FFT are heavily drowning below noise level. Here, we are only able to identify the first order reflections of silicon, i.e. information down to the 271 pm spacing. For comparison: an uncorrected Titan operated in STEM mode at 300 kV using an adequate illumination angle would be able to resolve the silicon dumbbells of 136 pm distance despite the present spherical aberration. Consequently, our experiment fails to demonstrate any improvement in resolution. Presently, the probe current in the aberration-corrected +1 order beam is not (yet) sufficient to enable high-quality HAADF STEM images.

5. Conclusions

We demonstrated that electron diffraction gratings can be used to correct the spherical aberration in a STEM. The utilization of the selected area aperture allows inspecting the Ronchigrams of the diffracted STEM probes individually to directly show the effect of aberration correction. This enables analysis and further tuning of the respective isolated STEM probe for further experiments and improvements. We were even able to use our GCOR to record C_S-corrected high-resolution HAADF STEM images, however, yet without any clear benefit for resolution improvement. In our experiment, the main advantage of C_S-correction – i.e. the use of a larger aperture for higher probe currents – was massively undermined by the very limited diffraction efficiency of our GCOR: although the usable aperture diameter doubled, the beam current dropped dramatically. The gain of usable aperture (four times the area) and the absolute diffraction efficiency $\eta_{abs,(+1)} = 2.5\%$ of the corrected probe effectively reduce the probe current to 10% with respect to the uncorrected reference setting.

For an Ångstrom-sized STEM probe, the geometric size of the electron source requires a strong demagnification into the object plane [34]. As a consequence, the limited brightness strongly limits the beam current within the illuminating angle as defined by the condenser aperture. For the brightness of 10^7 A/m^{2}srV (Schottky FEG) and an illumination half angle of 17.5 mrad at 300 keV electron energy not more than about 15 pA of beam current can be expected for a geometric source size of about 70 pm in the object plane. Consequently, the current of the +1 diffracted probe would result as 0.375 pA only, which clearly is too small for most high-resolution STEM experiments. Recent advances in grating processing, however, have shown promising improvements of diffraction efficiency already. An optimization of the grating thickness together with the trench depth allows improving the diffraction efficiency depending on electron energy [28]. Alternatively, since silicon nitride windows can be considered weak-phase objects to the electron beam, blazed gratings can be manufactured in order to boost the diffraction efficiency into the C_S-corrected probe and even suppress the transmitted beam [27,28]. Also, we propose using on-axis aberration correction by means of zone plates (circular gratings) [17,42] to further improve the usability, efficiency, and performance of holographic aberration correction.

Silicon nitride membranes are mainly used as support films for electron transparent samples in the transmission electron microscope (TEM), and consequently have to withstand relatively high dose rates. As an example, a high-resolution TEM illumination patch of 1 µm diameter and 1 nA of beam current results to a dose rate of 7913 e$^-$/s nm^2. In comparison, the total incident beam current of 15 pA for an Ångstrom-sized probe uniformly distributed over the grating of 35 µm radius results to dose rate of about 0.097 e$^-$/s nm^2 which is almost six orders of magnitude less compared to the TEM illumination. Accordingly, in our experiments we did not see any beam damage and charging effects on gratings that were placed into the condenser aperture. A high risk of damage only occurs during grating exchange due to mechanical accidents. However, if such a grating is positioned in the object plane for direct inspection with TEM illumination, considerable damage can be observed when using an excessively intense beam to illuminate the grating.

To conclude, there are several substantial advantages to summarize for a GCOR:

- Diffraction gratings are unbeatably inexpensive and easy to implement compared to multipole aberration correctors. The costs only comprise the silicon nitride windows and a day of FIB operation. Nano-patterning using lithographic techniques could also be used to mass-produce gratings. Such a low-cost solution could provide modest improvements in STEM capabilities of many instruments where multipole correctors are too expensive.
- A diffraction grating allows correcting any constant higher-order aberration not limited to the capabilities of multipoles.
- Other phase profiles (even non-analytic) can be superposed onto the aberration-correcting hologram for fancy novel experimental ideas.

However, diffraction gratings also have some substantial drawbacks that are difficult to overcome. In fact, the advantages only become relevant once substantial problems related to the method have been solved:

- Additional apertures are needed to effectively remove the transmitted 0^{th}-order probe and the undesired -1-order probe. This can be ameliorated by the use of more precise blazed gratings that divert most beam intensity into the desired diffraction order. Alternatively, zone-plates could be used.
- Precise capabilities for aberration measurement require suitable beam tilt capabilities above the grating position, which are presently not sufficiently available.
- Though any aberration can be corrected, it has to be known precisely in advance to be manufactured into the grating. This is impossible in most cases, because residual aberrations are not reliably measurable before the dominating spherical aberration is corrected.
- Diffraction gratings for spherical aberration are very inflexible in terms of condenser settings: each aperture magnification requires its own diffraction grating with a dedicated grating constant c_G. The same is true for the microscope's accelerating voltage: each high-voltage would require a different grating geometry. Both, the grating constant c_g and the grating's thickness and trench depth, have to be optimized for every individual high tension.
- Inelastic interaction in the grating's silicon nitride membrane complicates the energy distribution in the STEM probes. This may significantly hamper some analytic applications.

Finally, the successful application of a diffraction grating for aberration correction raises some interesting questions for future experiments:

- In light optics, diffraction gratings even allow correcting the chromatic aberration [43,44]. In future work, we propose to explore this idea for electrons as well.
- An aberration-correcting grating could also be used in a TEM to effectively correct the spherical aberration on the imaging side of an electron microscope. Our initial attempt to use gratings placed into the objective aperture for post-specimen, image-side aberration correction showed

that diffracted images of the specimen could not be isolated from one another using standard TEM configurations. This problem might be possible to solve either using efficient blazed aberration-correcting gratings or on-axis zone plate geometries.

Acknowledgments

Work by M.L. and P.E. at the Molecular Foundry was supported by the Office of Science, Office of Basic Energy Sciences of the U.S. Department of Energy under Contract No. DE-AC02—05CH11231. Work by B.M. and J.P. was supported by the U.S. Department of Energy (DOE), Office of Science, Basic Energy Sciences (BES) under Award # DE-SC0010466. We gratefully acknowledge the help of Josh Razink and the use of CAMCOR facilities at University of Oregon, which have been purchased with a combination of federal and state funding. M.L. gratefully acknowledges fruitful discussions with Dr. Peter Hartel (CEOS, Germany).

Disclosure of Financial Interests

M.L. is employed and paid by Corrected Electron Optical Systems GmbH (Heidelberg, Germany), a privately owned SME that develops and manufactures multipole aberration correctors.

References

[1] M. Haider, H. Rose, S. Uhlemann, E. Schwan, B. Kabius, K. Urban, Electron Microscopy Image Enhanced. Nature 392 (1998), 768-769.

[2] N. Dellby, O. L. Krivanek, P. D. Nellist, P. E. Batson & A. R. Lupini, Progress in aberration corrected scanning transmission electron microscopy. Journal of Electron Microscopy 50 (2001), 177-185.

[3] C.L. Jia, S.B. Mi, K. Urban, I. Vrejoiu, M. Alexe, and D. Hesse, Atomic-scale study of electric dipoles near charged an uncharged domain walls in ferroelectric films, Nature Materials 7 (2008) 57.

[4] M.C. Scott, C.-C. Chen, M. Mecklenburg, C. Zhu, R. Xu, P.A. Ercius, U. Dahmen, B.C. Regan, J. Miao, Electron tomography at 2.4-ångström resolution, Nature 483 (2012), 444–447.

[5] O.L. Krivanek, M.F. Chisholm, V. Nicolosi, T.J. Pennycook, G.J. Corbin, N. Dellby, M.F. Murfitt, C.S. Own, Z.S. Szilagyi, M.P. Oxley, S.T. Pantelides, S.J. Pennycook, Atom-by-atom structural and chemical analysis by annular dark-field electron microscopy, Nature 464 (2010), 571–574.

[6] R. Ishikawa , E. Okunishi, H. Sawada, Y. Kondo, F. Hosokawa, E. Abe, Direct imaging of hydrogen-atom columns in a crystal by annular bright-field electron microscopy, Nature Materials 10 (2011), 278-281.

[7] D.A. Muller, L. Fitting Kourkoutis, M. Murfitt, J.H. Song, H. Y. Hwang, J. Silcox, N. Dellby, O.L. Krivanek, Atomic-Scale Chemical Imaging of Composition and Bonding by Aberration-Corrected Microscopy, Science 319 (2008), 1073-1076.

[8] H. Müller, S. Uhlemann, P. Hartel, M. Haider, Advancing the Hexapole C_s-Corrector for the Scanning Transmission Electron Microscope, Microscopy and Microanalysis 12, Issue 06 (2006), 442-455.

[9] M. Haider, H. Müller, S. Uhlemann, J. Zach, U. Loebau, R. Hoeschen, Prerequisites for a Cc/Cs-corrected ultrahigh-resolution TEM, Ultramicroscopy 108 (2008), 167–178.

[10] J. Barthel, A. Thust, On the optical stability of high-resolution transmission electron microscopes, Ultramicroscopy 134 (2013), 6 - 17.

[11] M. Linck, B.J. McMorran, J.S. Pierce, P.A. Ercius, Aberration-corrected STEM by means of diffraction gratings, Microscopy and Microanalysis 20 S3 (2014), 946-947.

[12] B.J. McMorran, M. Linck, Device and method for creating Gaussian aberration-corrected electron beams, US Patent U.S. patent 9,240,255 (2014).

[13] B.R. Brown and A.W. Lohmann, Computer-generated Binary Holograms, IBM Journal of Research and Development 13 (1969), 160–168.

[14] D. C. O'Shea, T. J. Suleski, A. D. Kathman, and D. W. Prather, Diffractive Optics: Design, Fabrication, and Test, SPIE Publications (2003).

[15] L. Marton, Electron Interferometer, Phys. Rev. 85 (1952), 1057-1058.

[16] Y. Ito, A.L. Bleloch, J.H. Paterson, L.M. Brown, Electron Diffraction from Gratings Fabricated by Electron Beam Nanolithography, Ultramicroscopy 52 (1993), 347-352.

[17] Y. Ito, A.L. Bleloch, L.M. Brown, Nanofabrication of solid-state Fresnel lenses for electron optics, Lett.Nat.394 (1998), 49–52.

[18] J. Verbeeck, H. Tian, P. Schattschneider, Production and Application of Electron Vortex Beams, Nature 467 (2010), 301-304.

[19] B.J. McMorran, A.K. Agrawal, I.M. Anderson, A.A. Herzing, H.J. Lezec, J.J. McClelland, J. Unguris, Electron vortex beams with high quanta of orbital angular momentum, Science 331 (2011), 192-195.

[20] N.R. Heckenberg, R. McDuff, C.P. Smith, H. Rubinszteindunlop, M.J.Wegener, Laser-beams with phase singularities, Optical and Quantum Electronics 24 (1992), 951–962.

[21] L. Allen, M.W. Beijersbergen, R.J.C. Spreeuw, and J.P. Woerdman, Orbital angular-momentum of light and the transformation of laguerre-gaussian laser modes, Physical Review A45 (1992), 8185-8189.

[22] V.Y. Bazhenov, M.V. Vasnetsov, M.S. Soskin, Laser beams with screw dislocations in their wavefronts, JETP Letters 52 (1990), 429.

[23] B.J. McMorran, Electron Diffraction and Interferometry using Nanostructures, PhD-thesis (2009), University of Arizona.

[24] J. Verbeeck, H. Tian, A. Béché, Prospects for versatile phase manipulation in the TEM: A new way of producing electron vortex probes for STEM, Ultramicroscopy 113 (2012), 83-87.

[25] N. Voloch-Bloch,Y. Lereah,Y. Lilach, A. Gover, A. Arie, Generation of electron Airy beams, Nature 494 (2013), 331–335.

[26] R. Shiloh, Y. Lereah, Y. Lilach, A. Arie, Sculpturing the electron wave function using nanoscale phase masks, Ultramicroscopy 144 (2014), 26-31.

[27] V. Grillo, G.C. Gazzadi, E. Karimi, E. Mafakheri, R.W. Boyd, S. Frabboni, Highly efficient electron vortex beams generated by nanofabricated phase holograms. Applied Physics Letters 104 (2014), 043109.

[28] T.R. Harvey, J.S. Pierce, A.K. Agrawal, P.A. Ercius, M. Linck, B.J. McMorran, Efficient diffractive phase optics for electrons. New J. Phys. 16 (2014), 093039.

[29] B.J. McMorran, T. Harvey, J. Perry-Houts, S. Cabrini, A.K. Agrawal, H. Lezec, Sculpting Electron Beam Profile and Phase with Nanofabricated Diffractive Optics, The 56th International Conference on Electron, Ion, and Photon Beam Technology and Nanofabrication (EIPBN), 2012.

[29b] H. Lichte, Electron Holography Approaching Atomic Resolution, Ultramicroscopy 20 (1986), 293-304.

[30] B. Barwick, G. Gronniger, L. Yuan, S.-H. Liou, H. Batelaan, A measurement of electron-wall interactions using transmission diffraction from nanofabricated gratings, Journal of Applied Physics 100 (2006), 074322–074322–14.

[31] B.J. McMorran, J.D. Perreault, T.A. Savas, A.D. Cronin, Diffraction of 0.5 keV electrons from free-standing transmission gratings, Ultramicroscopy 106 (2006), 356-364.

[32] B.J. McMorran, D. Wanegar, A.D. Cronin, Low Energy Electron Holography of Charged Tip, Microscopy and Microanalysis 14 (2008), 350–351.

[33] B. J. McMorran, A. D. Cronin, An electron Talbot interferometer, New J. Phys. 11 (2009), 033021.

[34] E.J. Kirkland, Advanced Computing in Electron Microscopy, Second Edition, Springer New York, Dordrecht, Heidelberg, London (2010), ISBN 978-1-4419-6532-5, e-ISBN 978-1-4419-6533-2, DOI 10.1007/978-1-4419-6533-2.

[35] M.J. Hÿtch, E. Snoeck, R. Kilaas, Quantitative measurement of displacement and strain fields from HRTEM micrographs.Ultramicroscopy 74 (1998), 131-146.

[36] J.M. Cowley, Electron diffraction phenomena observed with a high-resolution STEM, J.Electron.Microsc.Tech.3 (1986), 25-44.

[37] O.L. Krivanek, N. Dellby, A.R. Lupini, Towards sub-Å electron beams, Ultramicroscopy 78 (1999), 1-11.

[38] M. Haider, H. Müller, S. Uhlemann, Present and Future Hexapole Aberration Correctors for High-resolution Electron Microscopy, Advances in Imaging and Electron Physics, Vol.153 (2008), 43-119.

[39] M. Haider, P. Hartel, H. Müller, S. Uhlemann, J. Zach, Current and Future aberration correctors for the improvement of resolution in electron microscopy, Phil.Trans.R.Soc. A367, Issue 1903 (2009), 3665.

[40] O.L. Krivanek, G.J. Corbin, N. Dellby, B.F. Elston, R.J. Keyse, M.F. Murfitt, C.S. Own, Z.S. Szilagyi, J.W. Woodruff, An electron microscope for the aberration-corrected era, Ultramicroscopy 108 (2008), 179-195.

[41] F. Hosokawa, H. Sawada, Y. Kondo, K. Takayanagi, K. Suenaga, Development of Cs and Cc correctors for transmission electron microscopy, Microscopy 62 (2013), 23-41.

[42] R. Shiloh, R. Remez, A. Arie, Prospects for electron beam aberration correction using sculpted phase masks, Ultramicroscopy 163 (2016), 69-74.

[43] H. Madjidi-Zolbanine, C. Froehly, Holographic correction of both chromatic and spherical aberrations of single glass lenses, Applied Optics 18 (1979), 2385.

[44] I. Weingärtner, K.-J. Rosenbruch, Chromatic Correction of Two- and Three-element Holographic Imaging Systems, Optica Acta: International Journal of Optics 29 (1982), 519–529.

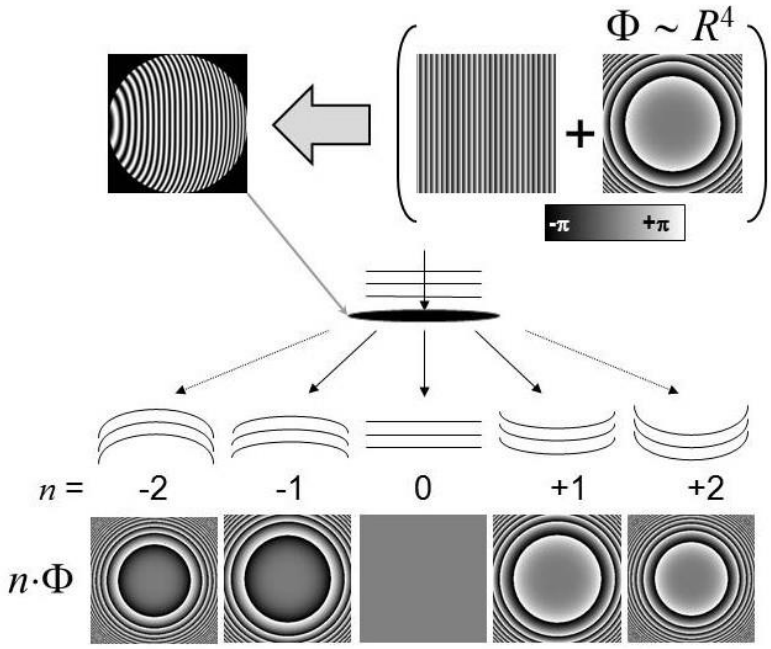

Figure 1: A line grating illuminated with a plane wave diffracts into multiple diffraction orders *n*. If an additional phase shift is superimposed to the linear phase shift of the grating lines, this phase shift in multiples of *n* can be found on the wave front of the *n*-th diffracted wave. Here, the parabolic phase shift of a spherical aberration is used for illustration.

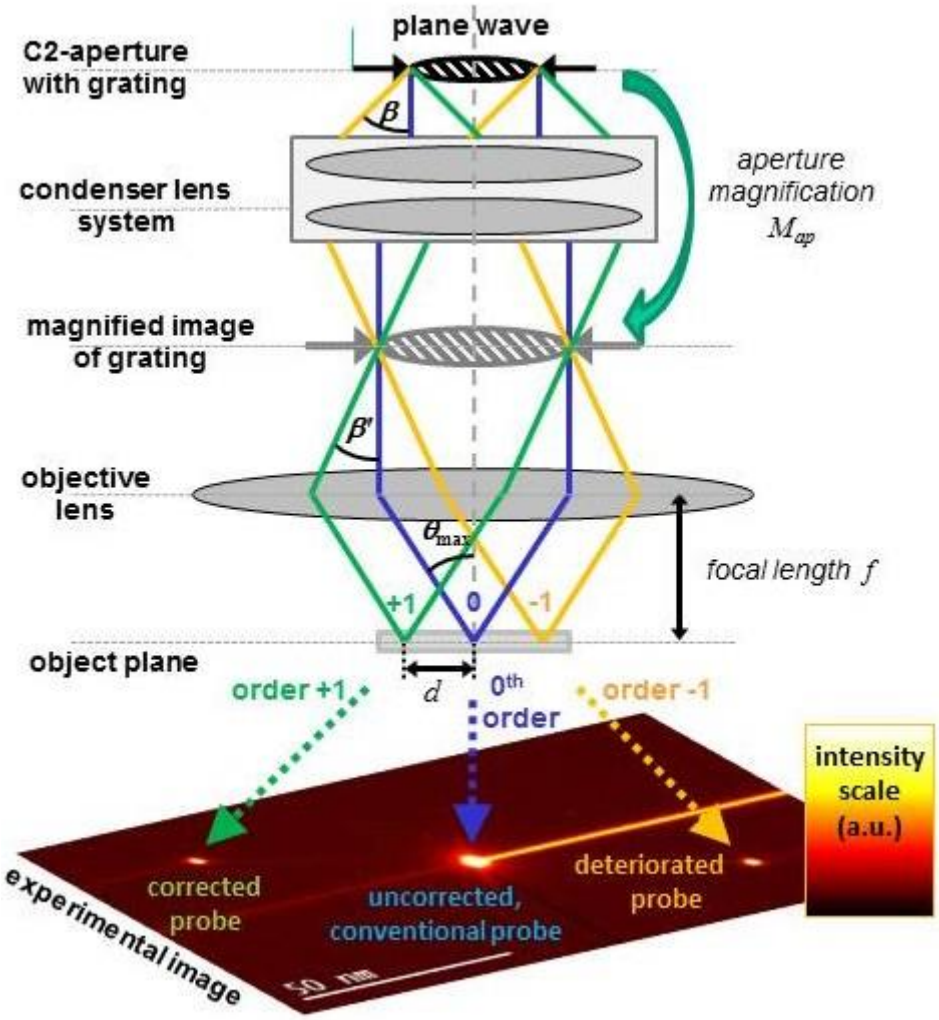

Figure 2: The condenser lens system images the diffraction grating from the probe forming condenser aperture to the front focal plane of the probe-forming objective lens. The corresponding aperture magnification M_{ap} magnifies the first-order diffraction angle β to β'. In the object plane the objective lens forms three main probes of probe angle θ_{max} which are separated by the distance d. In the experimental image the three probes are separated by about 50 nm; higher diffraction orders are very weak and can be ignored.

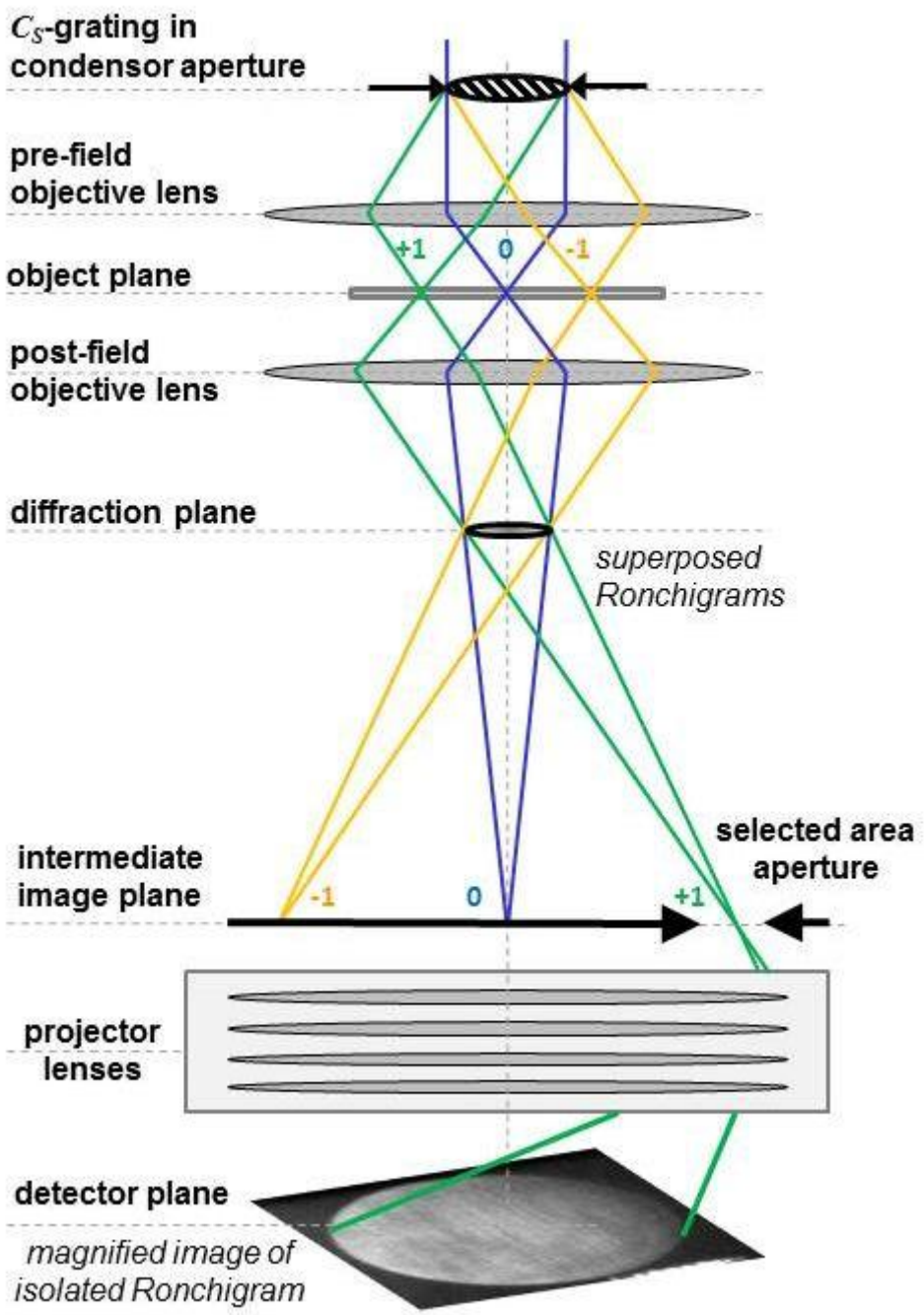

Figure 3: The diffraction patterns of the three probes are superimposed with each other in the diffraction plane. The Ronchigrams of the individual probes can be selected by isolating an individual probe using the selected area aperture. In the subsequent diffraction plane only the Ronchigram of the isolated probe can be observed. This allows e.g. analyzing the individual probe for further alignment purpose.

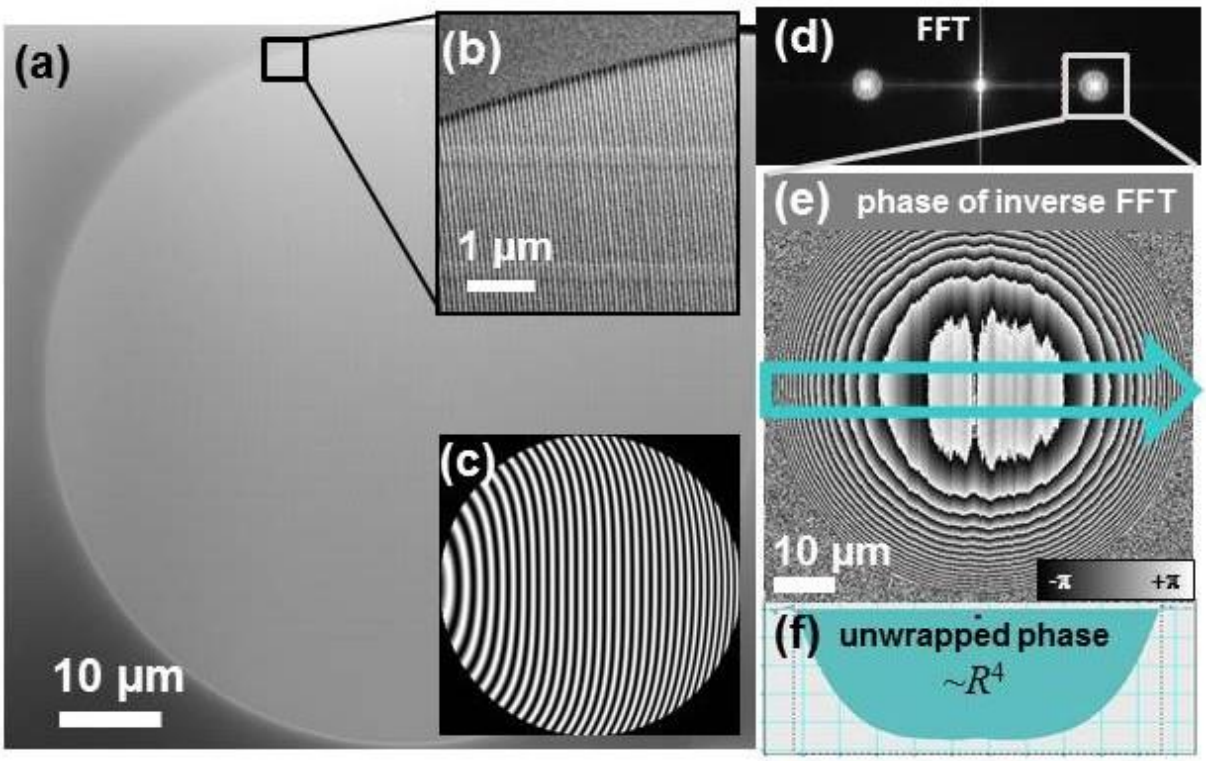

Figure 4: The SEM image (a) shows an overview of the complete diffraction grating for C_S-correction. The magnified subarea (b) exhibits the bending of the grating lines similar to the exaggerated model (c). Fourier analysis (d) allows reconstructing the geometric phase of the grating (e). The unwrapped phase profile (f) confirms the power-of-four behavior of the grating's phase shift.

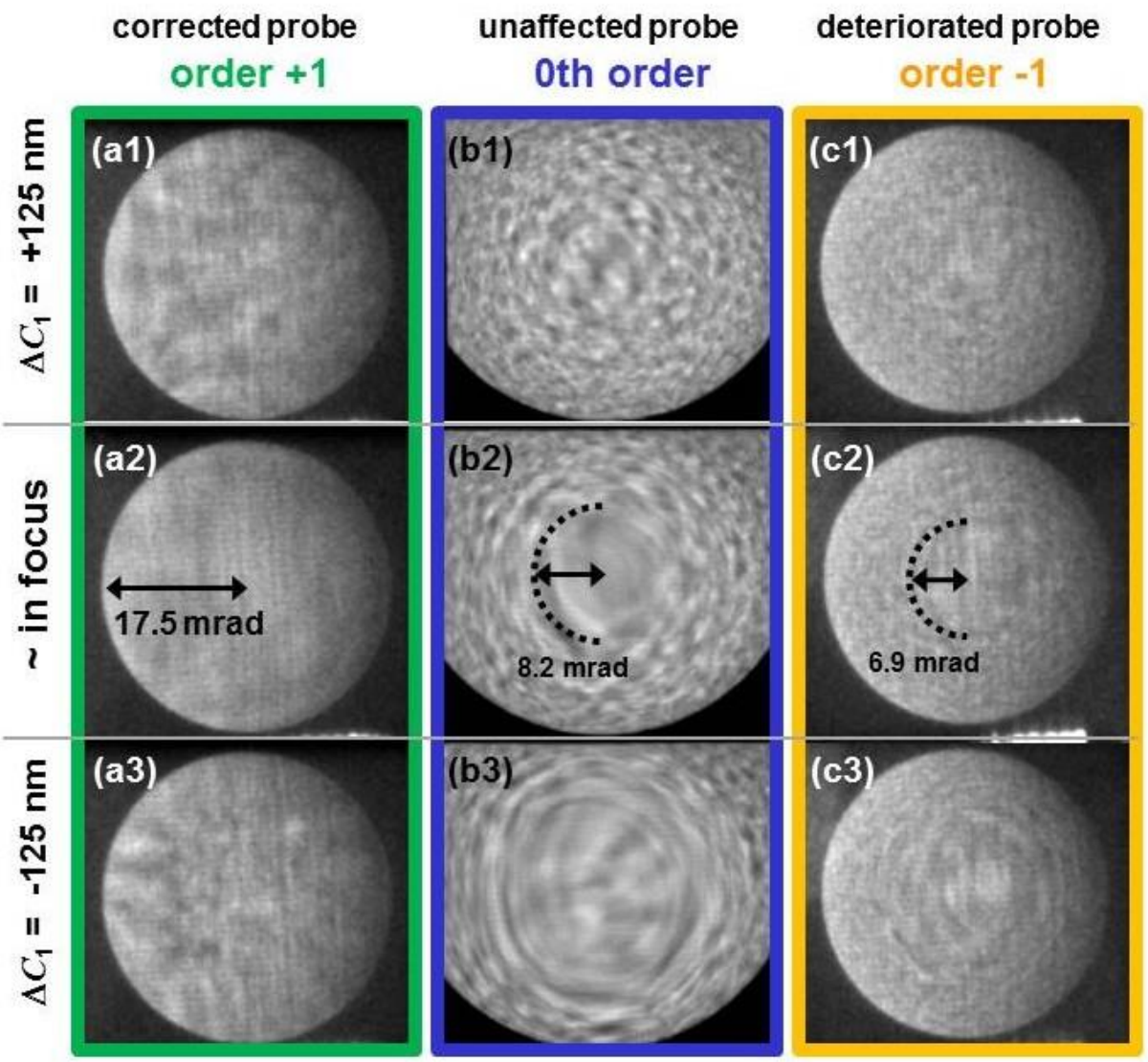

Figure 5: The isolated Ronchigrams of the C_S-corrected +1 order beam (a), the transmitted 0th order beam (b) and the twice-aberrated -1 order beam (c) allow analyzing the remaining spherical aberration. The focused Ronchigram is widely flat for the corrected beam (a2), whereas orders zero (b2) and -1 (c2) have considerably smaller flat areas in the Ronchigrams due to presence of millimeter sized spherical aberration. The Ronchigrams that are over- and underfocused by about 125 nm show the well-known behavior for a C_S-corrected probe (a1-a3) as well as for the aberrated, transmitted probe (b1-b3) and the deteriorated -1 probe (c1-c3), respectively.

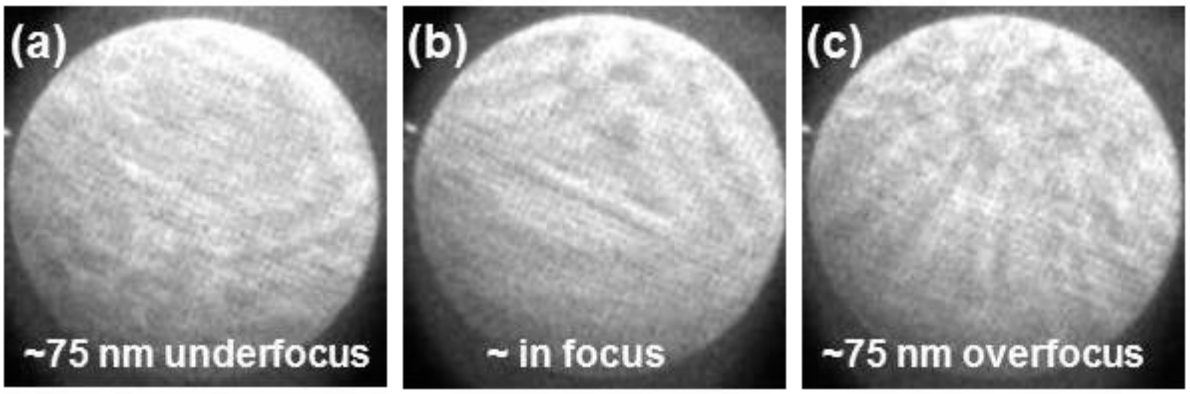

Figure 6: A dominating coma effect can be observed in the C_S-corrected "+1"-order Ronchigram, if the grating is misaligned w.r.t. to axis of the objective lens. The three Ronchigrams (a), (b) and (c) resemble a focus series with -75 nm, 0 nm and +75 nm of defocus, respectively.

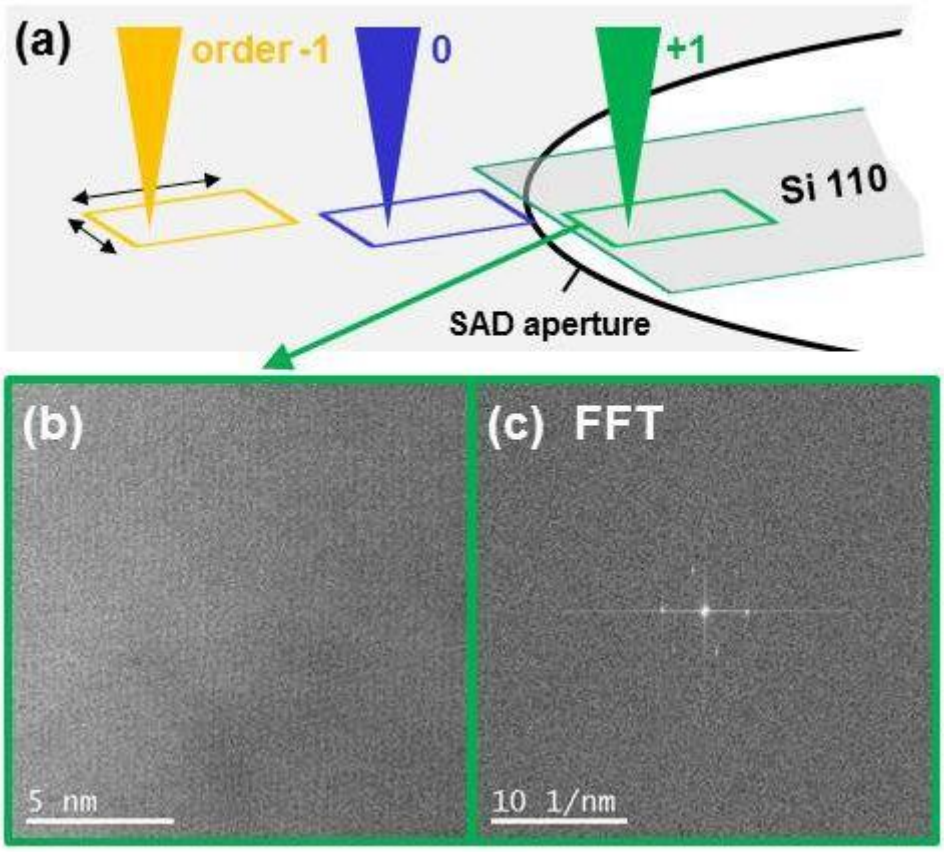

Figure 7: (a) The three probes are scanned simultaneously during STEM acquisition; hence the collected HAADF signal will be a superposition of three scanned areas. This can be overcome by scanning near the edge of the sample so that only one beam interacts with the sample and/or separating the scan area by means of a selected area aperture in the intermediate image plane. (b) The HAADF STEM image from our GCOR, i.e. the aberration-corrected +1 probe, is extremely noisy due to the small probe current. Nevertheless, the FFT (c) reveals high-resolution information up to the 271 pm reflection.